DocuServe

Electronic Delivery Cover Sheet

WARNING CONCERNING COPYRIGHT RESTRICTIONS

The copyright law of the United States (Title 17, United States Code) governs the making of photocopies or other reproductions of copyrighted materials. Under certain conditions specified in the law, libraries and archives are authorized to furnish a photocopy or other reproduction. One of these specified conditions is that the photocopy or reproduction is not to be "used for any purpose other than private study, scholarship, or research". If a user makes a request for, or later uses, a photocopy or reproduction for purposes in excess of "fair use", that user may be liable for copyright infringement. This institution reserves the right to refuse to accept a copying order if, in its judgment, fulfillment of the order would involve violation of copyright law.

Caltech Library Services

Photoelectrochemical Behavior of Planar and Microwire-Array Si|GaP Electrodes

Nicholas C. Strandwitz, Daniel B. Turner-Evans, Adele C. Tamboli, Christopher T. Chen, Harry A. Atwater, and Nathan S. Lewis**

Gallium phosphide exhibits a short diffusion length relative to its optical absorption length, and is thus a candidate for use in wire array geometries that allow light absorption to be decoupled from minority carrier collection. Herein is reported the photoanodic performance of heteroepitaxially grown gallium phosphide on planar and microwire-array Si substrates. The n-GaP|n-Si heterojunction results in a favorable conduction band alignment for electron collection in the silicon. A conformal electrochemical contact to the outer GaP layer is produced using the ferrocenium/ferrocene (Fc^+/Fc) redox couple in acetonitrile. Photovoltages of ~750 mV under 1 sun illumination are observed and are attributed to the barrier formed at the (Fc^+/Fc)|n-GaP junction. The short-circuit current densities of the composite microwire-arrays are similar to those observed using single-crystal n-GaP photoelectrodes. Spectral response measurements along with a finite-difference-time-domain optical model indicate that the minority carrier diffusion length in the GaP is ~80 nm. Solid-state current–voltage measurements show that shunting occurs through thin GaP layers that are present near the base of the microwire-arrays. The results provide guidance for further studies of 3D multi-junction photoelectrochemical cells.

1. Introduction

The use of nano- and micro-structured semiconductors for photoelectrochemical and photovoltaic devices decreases the distance required for minority-carrier collection, and is thus of interest for increasing the efficiency and lowering the purity requirements of absorber materials.[1,2] Some morphologies, including microwire arrays, also allow for optical concentration and effective light absorption.[3–5] The effective microscopic current density at structured electrode surfaces is less than that of planar devices, thus decreasing the overpotential required to drive kinetically slow reactions (e.g., water splitting) at a rate that is equal to the solar photon flux. Functional semiconductor wire arrays can also be embedded in polymer films and physically removed from the growth substrate, enabling the production of flexible photovoltaic and/or photoelectrochemical devices.[6]

A critical figure of merit in a photosynthetic electrochemical cell is the overall voltage produced by the light-absorbing components of the system. For example, the prototypical water-splitting reaction requires at least ~1.7 V (inclusive of overpotential requirements) to drive a current density of ~10 mA cm^{-2}. Systems that produce overall photovoltages less than ~1.7 V will thus not yield any net current or chemical fuel, in contrast to electricity-generating photoelectrochemical (PEC) cells or photovoltaics. The generation of such large voltages in an efficient device is optimized by use of a tandem configuration, comprised of two semiconductors having different bandgaps (E_g), because a single-junction device that produces a sufficiently large photovoltage would absorb only a small fraction of the photons in the solar spectrum.[7,8] If Si (E_g = 1.1 eV) is used for the lower bandgap material,[9] a semiconductor with a bandgap of 1.6–2.3 eV is needed for the larger bandgap absorber to produce an optimal tandem structure.[8]

Gallium phosphide (E_g = 2.26 eV) is an interesting candidate for use as a wide bandgap absorber in tandem PEC cells. Open-circuit voltages of 1.2 V and 1.5 V have been observed for GaP-based semiconductor/liquid and p–n homojunctions, respectively.[10,11] Assuming perfect collection of all photoexcited minority carriers, GaP can provide current densities of ~10 mA cm^{-2} under Air Mass 1.5 (AM 1.5) illumination. An optimized GaP photoelectrode that is connected electronically in series with Si could therefore in principle achieve solar-to-hydrogen thermodynamic efficiencies of 12% under AM 1.5 illumination. Reducing the bandgap to ~1.8 eV, by alloying with In or As, would provide a theoretical solar-to-hydrogen efficiency of 27%.[8]

Dr. N. C. Strandwitz, Prof. N. S. Lewis
Beckman Institute and Kavli Nanoscience Institute
Division of Chemistry and Chemical Engineering
California Institute of Technology
1200 E. California Blvd, Pasadena CA 91125, USA
E-mail: nslewis@caltech.edu
Mr. D. B. Turner-Evans, Dr. A. C. Tamboli,
Mr. C. T. Chen, Prof. H. A. Atwater
Thomas J. Watson Laboratories of Applied Physics
California Institute of Technology
1200 E. California Blvd, Pasadena CA 91125, USA
E-mail: haa@caltech.edu

DOI: 10.1002/aenm.201100728

© 2012 WILEY-VCH Verlag GmbH & Co. KGaA, Weinheim

FULL PAPER

The microstructuring of GaP has proven to be important in achieving large quantum yields for carrier collection, due to the short minority-carrier diffusion lengths (L_d) of GaP. The light absorption depths for GaP (500 μm near E_g, 10 μm at 486 nm) are generally greater than L_d (6 μm–100 nm), resulting in low external quantum yields displayed by bulk GaP samples.[12–14] Routes to structuring GaP in photoelectrochemical cells have generally utilized anodic etching, which results in a disordered porous structure, and yields an increase in the photocurrent due to the enhanced carrier-collection efficiency.[15–17] In parallel with developments in silicon microwire arrays,[1,3,4,18] the study of ordered structures based on GaP wire arrays will thus enable a subsequent generation of microwire-based energy conversion materials, as well as provide a more detailed understanding of the minority carrier collection in structured GaP-based photoelectrodes.

One route to the microstructuring and integration of GaP into a tandem configuration would involve the deposition of GaP on a structured template material.[19] Si and GaP are nearly lattice matched (fractional lattice mismatch = 0.358%). High quality GaP can therefore be grown heteroepitaxially on Si, as has been reported using liquid phase epitaxy,[20] metal organic chemical vapor deposition (MOCVD),[19,21–23] chemical beam epitaxy,[24,25] and halide transport.[26,27] Heteroepitaxial growth strategies therefore can provide a route to planar and structured monolithic tandem photovoltaics and photoelectrochemical cells.[28]

We describe the photoelectrochemical performance of GaP-coated Si microwires, and compare their performance to GaP-coated planar Si samples as well as to commercial GaP single-crystal wafers. The n^+-Si substrates served as a scaffold for the heteroepitaxial growth of GaP. Due to the close alignment of the Si and GaP conduction bands, which have an electron affinity difference, ΔE_A, of ~0.1–0.25 eV, the Si should function as an electron collector when the composite photoelectrode is operated as a photoanode in contact with the ferrocenium/ferrocene (Fc^+/Fc) redox couple. External quantum yield measurements were performed to assess the carrier-collection efficiency in GaP|Si microwires relative to planar control samples. Full-field optical simulations were used to quantify the light absorption in the Si cores and in the GaP shells, and to estimate the minority-carrier diffusion lengths in this system.

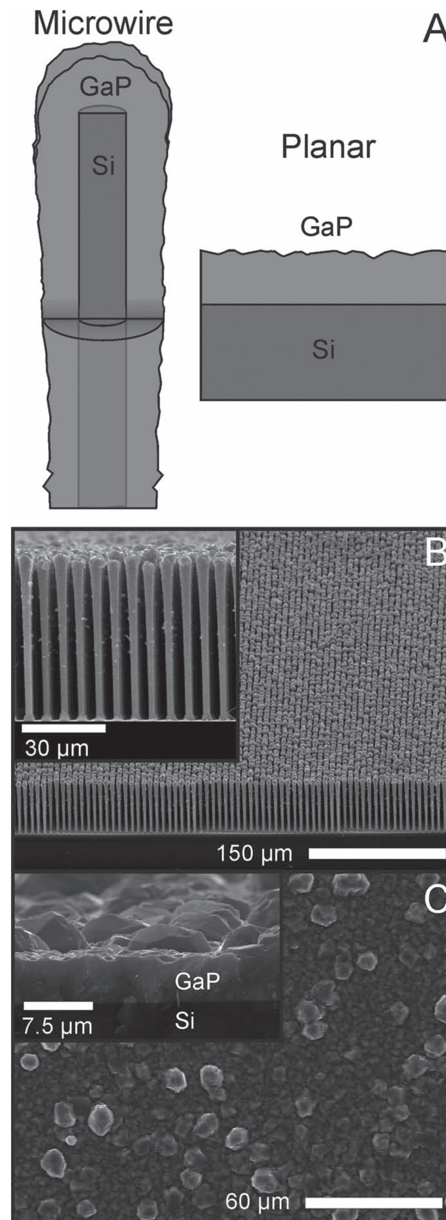

Figure 1. Graphical depiction (A) and scanning electron micrographs of GaP-coated Si microwire arrays (B) and of GaP-coated planar n^+-Si (C).

2. Results and Discussion

2.1. Structural and Photoelectrochemical Behavior of GaP|Si Photoelectrodes

Heteroepitaxial growth of GaP layers on vapor–liquid–solid (VLS) grown, degenerately doped n-type (n^+) Si microwire arrays, and on planar n^+-Si substrates, was performed by MOCVD. The GaP films coated the Si substrates conformally but exhibited significant surface roughness (**Figure 1**). The surface roughness resulted from defects that were produced during polar on non-polar heteroepitaxy, as opposed to indicating polycrystalline growth.[19] The thickness of the GaP layer on planar Si substrates was ~5 μm, as determined by cross-sectional scanning electron microscopy (SEM). The thickness of the GaP layer on Si microwire arrays varied from ~3.6 μm toward the top of the wires to 100–300 nm near the bases of the wires. The thinning of the GaP coating is ascribed to the depletion during MOCVD growth of the Ga and P precursors down the length of the wires.

Due to the similar electron affinities of GaP and Si, conduction band electrons should flow with minimal resistance from GaP to Si (**Figure 2**).[26,29,30] The Si cores of the microwires therefore should function as electron (majority carrier) collectors, in addition to being templates for structured growth.

To examine the properties of the MOCVD-deposited GaP and as well as of the GaP|Si junction, a liquid contact, consisting

© 2012 WILEY-VCH Verlag GmbH & Co. KGaA, Weinheim

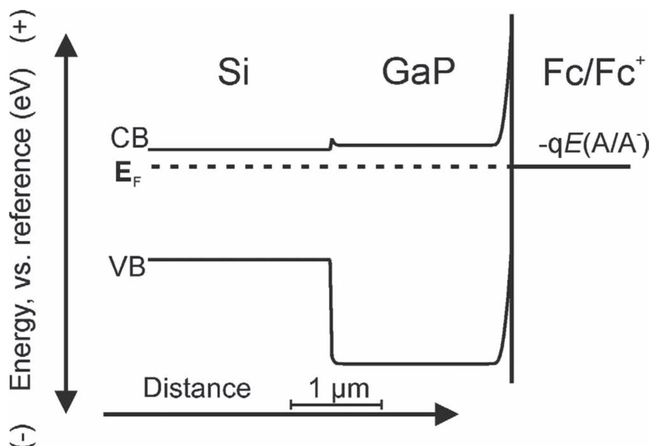

Figure 2. Simulated energy band diagram for the n+-Si | n-GaP | CH_3CN-ferrocenium/ferrocene system. (CB = conduction band, $\mathbf{E}_F$ = Fermi level, VB = valence band, $E(A/A^-)$ = solution redox potential)

of the Fc^+/Fc redox couple dissolved in acetonitrile (CH_3CN) with $LiClO_4$ as the supporting electrolyte, was used. The non-aqueous redox couple prevented corrosion of the semiconductor and insured intimate electrical contact to the structured photoelectrode surface.[31] The Fc^+/Fc couple produces a high barrier height with n-GaP.[11] Significant band bending at the n-Si|n-GaP interface is not expected, and thus any measured photoeffects can be attributed to the GaP shell as opposed to the degenerately doped n^+-Si core. Current density versus potential (J–E) data and photocurrent spectral response data (external quantum yield, Φ_{EXT}) for three sample types were measured, including GaP|Si microwire arrays, planar GaP|Si electrodes, and commercial GaP single-crystals (**Figure 3** and **Table 1**).

Under illumination with 100 mW cm^{-2} of ELH-type W-halogen illumination, all of the samples displayed large open-circuit voltages (V_{oc}), and exhibited anodic photocurrent (Figure 3). GaP|Si microwire and planar samples exhibited V_{oc} values of 750 ± 90 and 970 ± 60 mV, respectively. Commercial single-crystal n-GaP samples yielded V_{oc} values of 1.1 V. The magnitude of the voltage values is evidence that the observed photovoltages were due to the GaP absorber layers and not due to the photovoltaic properties of the n^+-Si substrates, which displayed V_{oc} values in contact with this redox system of <250 mV. The small voltage observed in Si samples that did not have GaP coatings was a consequence of doping-induced degradation prior to GaP heteroepitaxy.

The open-circuit voltages were ~220 mV smaller in GaP|Si microwire samples than in planar GaP|Si controls, due to increased dark current. The dark current generally scales linearly with the junction area. The GaP|Si microwire electrodes exhibited a geometric roughness factor (actual surface area/projected surface area) of ~10. This increase in roughness factor should therefore result in a 10-fold increase in dark current, and should thus lower the V_{oc} by ~60 mV, as opposed to the observed decrease of 220 mV (vide infra).

Planar GaP|Si samples exhibited short-circuit current densities (J_{sc}) of 0.27 mA cm^{-2}. Microwire array GaP|Si samples

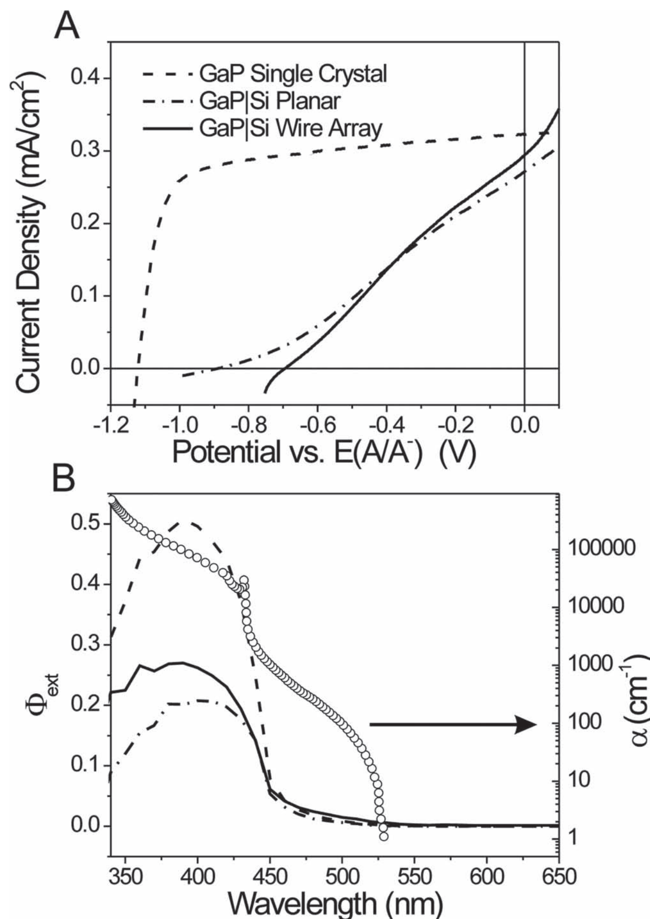

Figure 3. A) Photoelectrochemical current density vs potential data for planar GaP|Si junctions (dot-dashed curve), GaP|Si microwire arrays (solid curve), and commercial single-crystal n-GaP (dashed curve). The solution consisted of 50 mM ferrocene, 5.0 mM ferrocenium tetrafluoroborate, and 1.0 M lithium perchlorate in acetonitrile. B) External quantum yield (Φ_{EXT}) as a function of illumination wavelength (left), and absorption coefficient for GaP (right, open circles).[40,41]

displayed a slightly larger J_{sc} of 0.29 mA cm^{-2}. Commercial single-crystals exhibited the highest current densities, with J_{sc} = 0.32 mA cm^{-2}. Thus, all of the samples showed similar photocurrent densities despite the fact that the MOCVD-grown GaP samples had nominal absorber layer thicknesses of only ~4–5 μm, as compared to the >10 μm absorption length in GaP.

Table 1. Open-circuit voltage, short-circuit current density, fill factor, and energy conversion efficiency values for commercial single-crystal GaP wafers, planar GaP|Si and microwire-array GaP|Si samples. Voltages were measured using a high-impedance voltmeter.

Sample	GaP Wafer	GaP|Si Planar	GaP|Si Wire
V_{oc} [mV]	1100 ± 20	970 ± 60	750 ± 90
J_{sc} [mA/cm^2]	0.32 ± 0.02	0.27 ± 0.05	0.29 ± 0.05
ff	0.74 ± 0.02	0.21 ± 0.02	0.26 ± 0.03
η [%]	0.26 ± 0.02	0.05 ± 0.02	0.05 ± 0.02

© 2012 WILEY-VCH Verlag GmbH & Co. KGaA, Weinheim

These low J_{sc} values are consistent with the short minority-carrier diffusion length in GaP. Additionally, in the case of the wire arrays, parasitic absorption of light by the Si cores will decrease the measured photocurrent density.

The GaP|Si photoelectrodes displayed significant series resistance. The dark current density of the microwire samples was much larger than that observed in planar controls, and did not saturate at high bias (Supporting Information). Consequently, the energy conversion efficiencies (η) were lower for GaP|Si samples than for commercial n-GaP single-crystals. The smaller efficiency is attributed largely to the smaller fill factors for the heteroepitaxial GaP|Si samples (ff = 0.23) as compared to GaP single-crystals (ff = 0.74).

Figure 3B displays the external quantum yield (Φ_{EXT}) at normal incidence as a function of illumination wavelength of each of the samples. No photocurrent was observed at wavelengths (λ), longer than 550 nm, indicating that the Si did not contribute to the photocurrent. This observation is consistent with the >600 mV photovoltages that were measured under broadband illumination. The lack of photocurrent at λ >550 nm is also consistent with the relative band alignment, which implies the presence of a large barrier to holes in Si at the GaP|Si interface.[29] Small (0.01) Φ_{EXT} values at low photon energies were observed for all samples, consistent with the short value of L_d relative to the light absorption length of GaP. In the indirect-bandgap excitation regime (550–460 nm), as well as in most of the direct-bandgap excitation regime (λ < 430 nm), the wire array samples exhibited larger Φ_{EXT} values than did planar GaP|Si control samples. Integration of the external quantum yield of the GaP|Si microwire samples versus wavelength yielded an expected J_{sc} of ~0.32 mA cm^{-2} under AM 1.5 simulated illumination, in accord with the J_{sc} values observed experimentally.

The angular dependence of the incident light on Φ_{EXT} was investigated because off-normal incidence has been shown to increase the absorption (and thus increase Φ_{EXT}) in Si microwire arrays.[3,4] Increases in Φ_{EXT} in Si wire array samples have been attributed to increases in light scattering as well as to increases in the optical path length within the wires relative to illumination at normal incidence. The GaP|Si microwire samples displayed a minor decrease in Φ_{EXT} with increasing illumination angle, similar to the behavior observed for planar GaP|Si photoelectrodes (Supporting Information). Increases in Φ_{EXT} were presumably not observed because (1) the rough surface of the GaP-coated Si arrays scattered a large fraction of incoming light (vide infra) and (2) the interstitial spaces between the wires were predominantly occupied by GaP near the tops of the wires.[4] Specifically, the average interstitial distance between adjacent GaP surfaces between wires is 2.3 µm, whereas the distance between uncoated Si microwire surfaces is 4.7 µm. At normal incidence, light that would pass between the uncoated Si microwires is thus scattered and absorbed by the GaP|Si microwires. The decline in Φ_{EXT} is therefore attributable to slight increases in reflectivity at increasing angles of incidence, and to changes in the optical absorption profile of the composite microwires.

A finite difference time-domain (FDTD) model was used to simulate the light absorption at normal incidence, and to aid in understanding the photoelectrochemical properties of the GaP|Si microwires (**Figure 4**). A roughened surface geometry was used to mimic the actual surface of the composite photoelectrodes. A plane wave of 500 nm light was incident on the top of an individual wire with periodic side boundary conditions to account for coupling effects between wires in the square array. The 500 nm wavelength was used because it is in the indirect region of the GaP absorption spectrum, resulting in long light penetration depths and thus resulting in significant losses in photocurrent in planar GaP photoelectrodes that have short minority-carrier diffusion lengths. The FDTD simulations indicated that the composite GaP|Si microwire photoanodes should absorb a large fraction (88%) of the 500 nm light, with the percentage of 500 nm light absorbed in the GaP and Si

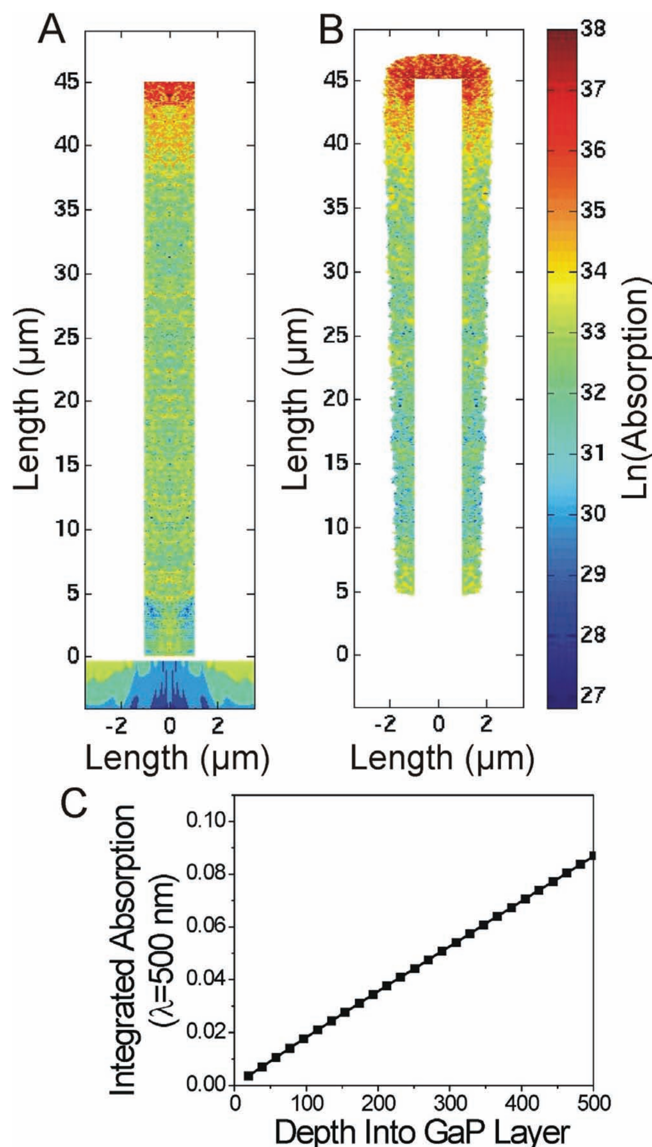

Figure 4. Simulated optical generation rate for 500 nm illumination normal to the top surface in the silicon core (A) and the gallium phosphide coating (B). Integrated absorption at 500 nm in the GaP layer. The fraction of absorption was integrated inwards from the outer GaP surface that was in contact with the redox couple.

© 2012 WILEY-VCH Verlag GmbH & Co. KGaA, Weinheim

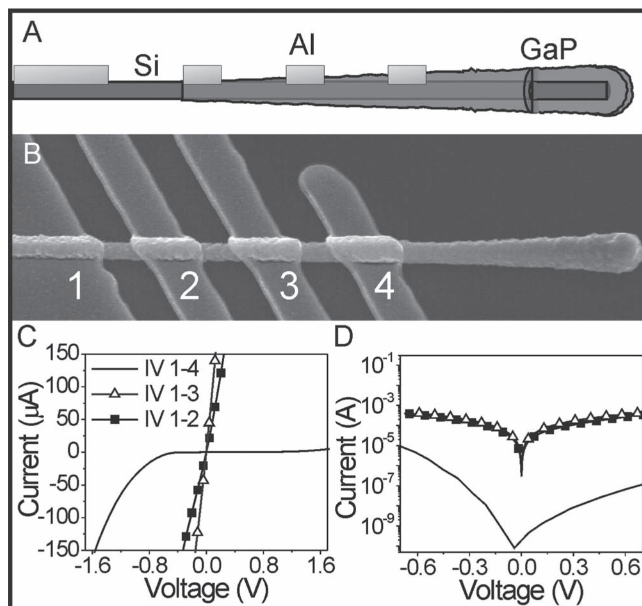

Figure 5. Single-wire current–voltage measurements. A) Schematic, and B) scanning electron microscope (SEM) image of a GaP|Si microwire with aluminum contacts. Current–voltage data (C, D) between the Si and GaP contacts as numbered in the figure. D) Plot shows an expanded semi-log plot of the data in (C).

calculated to be 20% and 68%, respectively. The majority of the light absorption was calculated to occur near the top of the wire, due to strong scattering arising from the microscale roughness of the MOCVD-grown GaP (Figure 4A,B)

Two observations can be made by comparing the photoelectrochemical data and the FDTD optical simulations. First, a significant percentage (68%) of high-energy photons (hν > 2.26 eV) were absorbed in the Si core, rather than the GaP shell, which resulted in a loss because photogenerated minority carriers in Si were not collected. Second, the effective carrier collection length, L_d, in the MOCVD GaP studied herein is ~80 nm. This value can be inferred from the amount of light absorption as a function of depth, radially integrated into the GaP layer from the outer surface (**Figure 5**C and Supporting Information). Specifically, at 80 nm depth, the FDTD simulations indicated that 1.5% of the 500 nm photons were absorbed, consistent with the Φ_{EXT} value that was measured at this wavelength (Φ_{EXT} = ~0.015). Such short L_d values are typical of GaP, and motivate future investigations of smaller absorber layer thicknesses as well as approaches to produce heteroepitaxial GaP with larger L_d values and to increase the absorption coefficient by band-structure modification.[32]

2.2. Investigations of the Reverse-Bias Shunting Current

The GaP|Si microwire array samples consistently exhibited large reverse-bias shunting currents. An increased shunting current decreases V_{oc}, and is therefore incompatible with efficient photoelectrochemical and photovoltaic systems. The explicit dependence of V_{oc} on the dark, reverse-saturation current density (J_0) is given by:[33]

$$V_{oc} = \frac{k_B T}{q} \ln\left(\frac{J_{ph}}{J_0}\right)$$

where k_B is Boltzmann's constant, T is the temperature, q is the unsigned charge on an electron, and J_{ph} is the photocurrent density.

The lack of shunting in planar control samples that had GaP layer thicknesses of >4 μm, suggests that the shunting in GaP|Si wire arrays occurred through thin GaP regions or through exposed n^+-Si regions that were located near the bases of the composite microwires. Three separate experiments were conducted to investigate the source of the shunting current.

First, a set of photoelectrodes that included GaP|Si microwires, planar n^+-Si, and planar GaP samples, were anodized under illumination in an aqueous phosphate buffer. This process formed a resistive silicon oxide on the exposed Si, thus passivating any exposed silicon surfaces. The samples were then immersed in 5 M HCl(aq), to remove any GaP surface regions that had been damaged by the anodization procedure. The etching step was preferential and did not etch the anodic silicon oxide, but, a small region of the Si may have been exposed by removal of the anodized GaP layer. The samples were then examined in contact with CH_3CN–Fc^+/Fc. Control n^+-Si samples exhibited very small reverse-bias current densities (<1μA cm^{-2} at 100 mV versus the Nernstian potential of the solution, $E(A/A^-)$). Large shunting currents were, however, observed for GaP|Si microwire samples (~300 μA cm^{-2} at 100 mV versus $E(A/A^-)$, Supporting Information). GaP and GaP|Si microwire samples exhibited similar photoresponses before and after the anodization/etching process. Thus, although this mild anodization and etching procedure formed a resistive barrier at exposed silicon surfaces, it did not adversely affect the GaP photoactivity or inhibit shunting.

Second, Si wires that had a 100 nm thick silicon oxide layer covering the lower 10 μm of the wire base were coated with GaP under MOCVD conditions that were identical to those used for the other MOCVD-deposited GaP samples (Supporting Information). SEM images of these samples indicated that the entire Si surface was covered with GaP. These samples also exhibited large shunting currents.

Spatially resolved, single-wire current–voltage (*I–V*) measurements were then obtained on solid-state devices that had been formed by evaporating Al contacts along the Si wire base and the GaP-coated region (Figure 5). Aluminum forms an ohmic contact to n^+-Si and a Schottky contact to n-GaP. This configuration was thus similar to the electrochemical experiments described above, except that Al was used as a local Schottky contact instead of CH_3CN-Fc^+/Fc acting as a conformal liquid contact. The current–voltage data measured between the Si contacts and thick (>1 um) GaP regions displayed resistive diode-like behavior, and showed small reverse-bias currents (Figure 5C, D). In contrast, the *I–V* data obtained between the Si contacts and thin (<300 nm) GaP regions exhibited an ohmic response, consistent with the shunting behavior that was observed for the liquid contacts.

 © 2012 WILEY-VCH Verlag GmbH & Co. KGaA, Weinheim

These observations suggest that the shunting in the microwire array samples occurred through thin GaP regions located near the bases of the wires. Previous studies of MOCVD-grown GaP on Si have shown that the GaP layers near the surface are highly doped n-type, due to diffusion of Si at the growth temperature.[23] High Si-doping of the n-GaP will result in a thin depletion region, allowing appreciable majority carrier tunneling through the barrier. Further, little is known about the effects of strain and crystallographic defects on photoelectrode behavior. Such phenomena are often present at GaP|Si interfaces[34] and are likely to be present in the composite GaP|Si microwire arrays.

3. Design Criteria

This work provides considerations for further development of tandem microwire devices for photovoltaic and PEC applications. Integration of compound semiconductors with silicon is one path to obtain systems that produce the photovoltages that are required for water splitting. We have demonstrated herein the integration of VLS-grown Si with GaP coatings, in an attempt to increase the available photovoltages relative to those produced by Si alone.

Although the study verified the concept, avenues to achieve significant improvements in the energy-conversion efficiency and overall device properties are clearly apparent. Increases in the overall fraction of short-wavelength absorption in the GaP layer could be achieved by decreasing the core diameter of the Si, increasing the thickness of the GaP layer, or changing the composition of the GaP layer to increase the absorption coefficient of the shell material. Increases in the thickness of the GaP layer will not, however, increase the quantum yield values, because of the short diffusion length of holes in GaP. The L_d values found in this work and by others[12,15–17] indicate that minority carriers that are generated more than ~100 nm from the junction are not collected. These findings therefore suggest that a GaP layer thickness of ~100 nm would be optimal from a carrier collection standpoint. However, a 100 nm GaP layer thickness would not allow for sufficient light absorption because 100 nm is much shorter than the absorption depth of GaP. Band-structure modification by incorporation of nitrogen,[32,35] indium,[36] or arsenic[12] would allow for increases in the absorption coefficient and possibly increases in L_d, although at a slight loss of V_{oc}. Varying the GaP composition, however, may increase the strain and consequently, the defect densities at the interface, due to an increase in the fractional lattice mismatch.

Shunting currents must also be considered because of their large impact on V_{oc}. In this heteroepitaxial system, the shunting currents could be reduced by making thicker and more uniform GaP layers or by reducing the growth temperature, thus minimizing the diffusion of Si into GaP. The shunting currents that may be induced by unintentional Si doping could also be minimized by avoiding the use of a Si template for radial growth. For example, the direct growth of GaP wire arrays by VLS methods might allow for the formation of axial junctions with Si, while precluding the radial diffusion of Si during growth.[37] Axial geometries will place the two absorbers optically in series, which is important for achieving spectral splitting of solar photons.

More complex systems, such as structures in which the Si core is used as a functional absorber, could generate an additional ~500 mV of photovoltage that would be added to the photovoltage generated by GaP. This tandem system requires a tunnel junction, or an ohmic contact, between the two semiconductors, but is another promising approach that could enable utilization of Si|GaP materials system in a solar-driven water-splitting assembly.

4. Conclusion

Si can be used as an electron collector for structured GaP absorbers. The external quantum efficiency was comparable for GaP|Si microwire arrays and for planar GaP|Si samples. Optical simulations were used in conjunction with the photocurrent spectral response data to estimate a minority-carrier collection length of ~80 nm in the MOCVD-grown GaP coatings. Active shunting pathways were investigated, and provided guidelines for further development of structured photoelectrodes. Our results indicate that high-efficiency GaP-based microwire arrays can be realized by increasing the minority carrier diffusion length and/or the absorption coefficient of the GaP layers.

5. Experimental Section

Acetonitrile was dried using a solvent purification system.[38] Ferrocene (Sigma Aldrich, 98%) was purified by sublimation. Ferrocenium tetrafluoroborate that was generated by the chemical oxidation of sublimed ferrocene was washed with diethyl ether and dried in vacuum. Lithium perchlorate (Sigma Aldrich, battery grade) was used as received. Gallium phosphide single-crystals were obtained from MTI (doping density (N_D) = $2–7 \times 10^{17}$ cm^{-3}).

Silicon microwires were grown by patterning 3 μm diameter holes in a photoresist layer (Shipley S1518) that had been spin-coated onto silicon substrates (3000 rpm, 60 s) that were coated with a 300 nm thick thermal oxide (obtained from Cemat Silicon, resistivity 0.005–0.018 Ω cm).[3] The thermal oxide was etched in buffered HF (aq., Transene) for 4 min, rinsed with water, and dried. Immediately after etching, 300 nm of Cu was deposited by thermal evaporation. Wire growth proceeded by heating a 1.2 cm by 1.5 cm sample to 1000 °C in flowing H_2 (500 sccm, 20 min) and then adding He bubbled through $SiCl_4$ (Strem 99.9999%) at 20 sccm for 20 min. No dopants were intentionally added during growth.

The microwires were cleaned[39] to remove residual copper metal, and were then doped n-type by in-diffusion of phosphorus. Copper was removed by immersing the sample sequentially in 5.7 M HF (5 s), freshly mixed $HCl:H_2O_2:H_2O$, 1:1:6 (20 min, 70 °C), 5.7 M HF (5 s), and then dried under a N_2(g) stream. The photoelectrodes were then etched in 4.3 M KOH(aq) for 40 s, thoroughly rinsed with water, and dried under a stream of N_2(g). Electrodes were doped with phosphorous using diffusion wafers (Saint Gobain, PH 1000N). The depth of P diffusion into the Si wire was calculated to be greater than the wire diameter, resulting in non-uniformly, but degenerately, doped n-type Si wire arrays.

GaP was grown by MOCVD on planar Si samples (Cemat Silicon, resistivity 0.005–0.018 Ω·cm) and on Si microwires. Immediately prior to deposition, the photoelectrodes were immersed in buffered HF for 10 s, rinsed with H_2O, and dried. Trimethylgallium and phosphine precursors were used for growth. An initial nucleation stage at 530 °C was followed by continued growth at 750 °C. The samples were grown n-type by fixing

© 2012 WILEY-VCH Verlag GmbH & Co. KGaA, Weinheim

the precursor V/III ratio at 80. Extrinsic dopants were not added during GaP growth.

GaP|Si photoelectrodes were fabricated by scratching In-Ga into the back side of the Si wafer, to form an ohmic contact. The chips were then attached to a coiled, tinned-Cu wire by application of Ag paste. The semiconductor electrode was then passed through a ¼ inch outer-diameter glass tube, and was sealed with epoxy (Hysol 1C and 9460) leaving only the semiconductor surface (Typical area ~0.05 cm^2), epoxy, and glass exposed to the solution. GaP single-crystals were contacted using In metal, and were annealed at 400 °C under forming gas (5% H_2(g) in N_2(g)) for 10 min. Prior to measurement, photoelectrodes were etched for 20 s with 5 M HCl (aq).

Single wire measurements were performed by photolithographically patterning Al contacts onto individual wires that had been deposited onto an insulating silicon nitride film on a Si substrate.[39] The composite microwires were removed from the growth substrate using a razor blade, dispersed in isopropanol, and spin-cast at 100–200 rpm onto the silicon nitride substrate. The sample was dried at 115 °C and was subsequently exposed to hexamethyldisilazane vapor for 2 min. LOR10A (Microchem) was then spin-cast (1500 rpm, 30 s) and baked at 180 °C for 5 min. S1813 (Microchem) was then spin-cast (3000 RPM, 30 s) and the sample was baked at 115 °C for 2 min. The sample was exposed to UV light (Karl Suss MA6) and developed in MF319 developer for 1.5–3 min. Al (1200 nm) was deposited by electron-beam evaporation and lift off was performed in PG Remover (Microchem) at 50 °C for 12 h. Current–voltage measurements were obtained using a Keithley 2602A Sourcemeter. Many samples (>20) were tested, with results shown for a single microwire. The data presented display the typical range of behaviors that were observed (ohmic and rectifying), depending on the thickness of the GaP layer that was contacted.

Current–voltage data were collected with, and without, 100 mW cm^{-2} of ELH-type W-halogen illumination in a stirred glass electrochemical cell placed in an Ar-filled glove box. The solution composition was 0.50 mM ferrocenium tetrafluoroborate, 20 mM ferrocene, and 1.0 M lithium perchlorate. A Pt mesh and a Pt wire were used as counter and reference electrodes, respectively. Spectral response data were collected under Ar(g) in a sealed glass cell that had a quartz window. The solution contained a low concentration of redox species (0.0050 mM ferrocenium, 0.20 mM ferrocene). Light intensities were calibrated with a Si photodiode (Thor Labs) that was placed at the same location in the cell as the photoelectrodes. Angle-dependent external quantum yield measurements were conducted using a side-facing electrode, illuminated with a spot size that was much larger, at all angles, than the exposed semiconductor surface. The effective light intensity thus decreased as $I_0 \cdot \cos(\theta)$, where I_0 is the illumination intensity at normal incidence and θ is the angle of the incident light relative to normal incidence ($\theta = 0°$ at normal incidence). This change in light intensity was factored into the calculation of the angle-dependent external quantum yields. Band diagrams were simulated using the Sentaurus Device software program from Synopsys Inc. The values used for the electron affinity ($\mathbf{E_A}$) and doping density (N_D) were: Si $N_D = 5 \times 10^{18}$ cm^{-3}, $\mathbf{E_A} = 4.05$ eV; GaP $N_D = 1 \times 10^{16}$ cm^{-3}, $\mathbf{E_A} = 4.05$ eV. The equilibrium band diagrams were calculated by solving the Poisson and electron/hole continuity equations in 1D.

Finite-difference time-domain simulations of the light absorption were carried out using Lumerical, a commercial finite-difference time-domain software package. The structural model was constructed to match the experimental SEM images, and consisted of a 45 μm tall Si wire on top of a Si substrate that was surrounded by GaP. Randomly oriented GaP squares (width = 500 nm) were placed inside an envelope function, to follow the overall shape and roughness of the actual wires. The top and bottom boundary conditions were set to produce perfectly matched absorbing layers, while the sides were periodic. A 500 nm plane-wave source was positioned 1 μm above the top of the wire. After completion of the simulation, the absorption was calculated as $1/2\ \omega\ \varepsilon''\ |E|^2$. The values were then normalized to the incident power and integrated inwards from the outer surface toward the Si core.

Supporting Information

Supporting Information is available from the Wiley Online Library or from the author.

Acknowledgements

We acknowledge the National Science Foundation (NSF) Center for Chemical Innovation (CHE-0802907) and DARPA for support. NCS acknowledges the NSF for an American Competitiveness in Chemistry postdoctoral fellowship (CHE-1042006). DBTE acknowledges the NSF for a Graduate Research Fellowship. The authors acknowledge helpful discussions from Dr. Chengxiang Xiang and Prof. Shannon W. Boettcher.

Received: November 29, 2011
Published online: June 15, 2012

[1] B. M. Kayes, H. A. Atwater, N. S. Lewis, *J. Appl. Phys.* **2005**, *97*, 114302.
[2] J. M. Spurgeon, K. E. Plass, B. M. Kayes, B. S. Brunschwig, H. A. Atwater, N. S. Lewis, *Appl. Phys. Lett.* **2008**, *93*, 032112.
[3] S. Boettcher, J. Spurgeon, M. Putnam, E. Warren, D. Turner-Evans, M. Kelzenberg, J. Maiolo, H. Atwater, N. Lewis, *Science* **2010**, *327*, 185–187.
[4] M. Kelzenberg, S. Boettcher, J. Petykiewicz, Turner-Evans, D. M. Putnam, E. Warren, J. Spurgeon, R. Briggs, N. Lewis, H. Atwater, *Nat. Mater.* **2010**, *9*, 239–244.
[5] M. Putnam, S. Boettcher, M. Kelzenberg, D. Turner-Evans, S. J. purgeon, E. Warren, R. Briggs, N. Lewis, H. Atwater, *Energy & Environ. Sci.* **2010**, *3*, 1037–1041.
[6] J. M. Spurgeon, S. W. Boettcher, M. D. Kelzenberg, B. S. Brunschwig, H. A. Atwater, N. S. Lewis, *Adv. Mater.* **2010**, *22*, 3277–3281.
[7] M. F. Weber, M. J. Dignam, *J. Electrochem. Soc.* **1984**, *131*, 1258–1265.
[8] J. R. Bolton, S. J. Strickler, J. S. Connolly, *Nature* **1985**, *316*, 495–500.
[9] S. W. Boettcher, E. L. Warren, M. C. Putnam, E. A. Santori, D. Turner-Evans, M. D. Kelzenberg, M. G. Walter, J. R. McKone, B. S. Brunschwig, H. A. Atwater, N. S. Lewis, *J. Am. Chem. Soc.* **2011**, *133*, 1216–1219.
[10] C. R. Allen, J.-H. Jeon, J. M. Woodall, *Solar Energy Materials and Solar Cells* **2010**, *9*, 2655–2658.
[11] C. M. Gronet, N. S. Lewis, *Nature* **1982**, *300*, 733–735.
[12] C. M. Gronet, N. S. Lewis, *J. Phys. Chem.* **1984**, *88*, 1310–1317.
[13] A. B. Ellis, J. M. Bolts, S. W. Kaiser, M. S. Wrighton, *J. Am. Chem. Soc.* **1977**, *99*, 2848–2854.
[14] M. L. Young, D. R. Wight, *J. Phys. D: Appl. Phys.* **1974**, *7*, 1824–1837.
[15] M. J. Price, S. Maldonado, *J. Phys. Chem. C* **2009**, *113*, 11988–11994.
[16] S. Yamane, N. Kato, S. Kojima, A. Imanishi, S. Ogawa, N. Yoshida, S. Nonomura, Y. Nakato, *J. Phys. Chem. C* **2009**, *113*, 14575–14581.
[17] D. Vanmaekelbergh, B. H. Erné, C. W. Cheung, R. W. Tjerkstra, *Electrochimica Acta* **1995**, *40*, 689–698.
[18] C. E. Kendrick, H. P. Yoon, Y. A. Yuwen, G. D. Barber, H. Shen, T. E. Mallouk, E. C. Dickey, T. S. Mayer, J. M. Redwing, *Appl. Phys. Lett.* **2010**, *97*, 143108.
[19] A. C. Tamboli, M. Malhotra, G. M. Kimball, D. B. Turner-Evans, H. A. Atwater, *Appl. Phys. Lett.* **2010**, *97*, 221914–3.
[20] S. R. Huang, Xuesong Lu, A. Barnett, R. L. Opila, *34th IEEE PVSC* **2009**, 1436–1438.
[21] T. Soga, T. Suzuki, M. Mori, Z. K. Jiang, T. Jimbo, M. Umeno, *J. Cryst. Growth* **1993**, *132*, 414–418.
[22] V. K. Dixit, T. Ganguli, T. K. Sharma, R. Kumar, S. Porwal, V. Shukla, A. Ingale, P. Tiwari, A. K. Nath, *J. Cryst. Growth* **2006**, *293*, 5–13.
[23] J. Andre, J. Hallais, C. Schiller, *J. Cryst. Growth* **1975**, *31*, 147–157.

© 2012 WILEY-VCH Verlag GmbH & Co. KGaA, Weinheim

[24] K. J. Bachmann, *J. Vac. Sci. Technol. B***1996**, *14*, 3019–3029.
[25] V. Narayanan, N. Sukidi, C. Hu, N. Dietz, K. J. Bachmann, S. Mahajan, S. Shingubara, *Mat. Sci. Eng. B* **1998**, *54*, 207–209.
[26] G. Zeidenbergs, R. L. Anderson, *Solid-State Electronics* **1967**, *10*, 113–123.
[27] T. Katoda, M. Kishi, *J. Electron. Mat.* **1980**, *9*, 783–796.
[28] O. Khaselev, J. Turner, *Science* **1998**, *280*, 425–427.
[29] I. Sakata, H. Kawanami, *Appl. Phys. Express* **2008**, *1*, 091201.
[30] T. Katoda, M. Kishi, *J. Electron. Mat.* **1980**, *9*, 783–796.
[31] J. Maiolo, B. Kayes, M. Filler, M. Putnam, M. Kelzenberg, H. Atwater, N. Lewis, *J. Am. Chem. Soc.* **2007**, *129*, 12346–12348.
[32] B. Fluegel, Y. Zhang, J. F. Geisz, A. Mascarenhas, *Phys. Rev. B* **2005**, *72*, 073203.
[33] S. M. Sze, K. K. Ng, *Physics of Semiconductor Devices*, 3rd ed., Wiley-Interscience, **2006**.
[34] V. Narayanan, S. Mahajan, K. J. Bachmann, V. Woods, N. Dietz, *Phil. Mag. A* **2002**, *82*, 685.
[35] T. G. Deutsch, C. A. Koval, J. A. Turner, *J. Phys. Chem. B* **2006**, *110*, 25297–25307.
[36] R. J. Nelson, N. Holonyak Jr., *J. Phys. Chem. Sol.* **1976**, *37*, 629–637.
[37] K. A. Dick, K. Deppert, T. Mårtensson, W. Seifert, L. Samuelson, *J. Cryst. Growth* **2004**, *272*, 131–137.
[38] A. B. Pangborn, M. A. Giardello, R. H. Grubbs, R. K. Rosen, F. J. Timmers, *Organometallics* **1996**, *15*, 1518–1520.
[39] M. D. Kelzenberg, D. B. Turner-Evans, B. M. Kayes, M. A. Filler, M. C. Putnam, N. S. Lewis, H. A. Atwater, *Nano Lett.* **2008**, *8*, 710–714.
[40] D. E. Aspnes, A. A. Studna, *Phys. Rev. B* **1983**, *27*, 985.
[41] P. J. Dean, *J. Appl. Phys.***1967**, *38*, 3551.

© 2012 WILEY-VCH Verlag GmbH & Co. KGaA, Weinheim